Two-wavelength phase shifting interferometry

Yeou-Yen Cheng and James C. Wyant

This paper describes a technique that combines ideas of phase shifting interferometry (PSI) and two-wavelength interferometry (TWLI) to extend the phase measurement range of conventional single-wavelength PSI. To verify theoretical predictions, experiments have been performed using a solid-state linear detector array to measure 1-D surface heights. Problems associated with TWLPSI and the experimental setup are discussed. To test the capability of the TWLPSI, a very fine fringe pattern was used to illuminate a 1024 element detector array. Without temporal averaging, the repeatability of measuring a surface having a sag of ~100 μm is better than 25-Å (0.0025%) rms.

I. Introduction

New microcomputers, state-of-the-art solid-state detector arrays, and high quality piezoelectric transducers (PZT) make phase shifting interferometry (PSI)[1,2] a very important technique in interferometric optical testing. There are several well-known advantages of PSI. For example, (1) fast measurement speed, (2) high phase-measurement accuracy, (3) good results even when the fringe contrast is poor, (4) phase measurements independent of spatial intensity variation across the wave front, (5) the phase is obtained at a fixed grid of data points, and (6) polarity of wave front can be determined.

The basic idea of PSI is that, if the phase difference between the two interfering beams is made to vary in some known manner, such as changing in discrete steps or changing linearly with time, three or more measurements of the intensity distribution across the pupil for different phase differences between the interfering beams can be used to determine the phase distribution across the pupil.

In the situation of testing surface roughness while no tilt fringes are present, the PSI proved to be a very high precision measurement technique where the precision of measurement is in the range from $\lambda/100$ to $\lambda/1000$ peak–valley. If two or more interference fringes are present, a major problem with PSI is obtaining the proper phase shift between data frames. If the phase shift is incorrect a nearly sinusoidal phase error of twice the spatial frequency of the interference fringes is obtained as illustrated in Fig. 1 for the case where the phase shift between frames is supposed to be 90° but is actually 88°. A convenient way of reducing this error is to make two sets of measurements, where the initial phase difference between the two sets differs by ~90° and then average the two sets of measurements.

In PSI the phase distribution across the interferogram is measured modulo 2π. Thus the measured phase distribution will contain 2π discontinuities. As long as the slope of the wave front being measured is small enough so that the phase changes by $<\pi$ between adjacent detector pixels, the phase discontinuities can be removed. The procedure is to check to see if the measured phase change between adjacent pixels is $>\pi$, and if it is, an integer number of 2π is added or subtracted to the measured phase so the phase difference between adjacent pixels is always $<\pi$.

If the slope of the test surface is steep enough that the phase change between any adjacent pixels is larger than π, the 2π ambiguity problem will ruin the result of the phase measurement. This problem sets a limit to the phase measurement range of single-wavelength PSI. Of course, one can use a higher resolution detector array, but there is a trade-off between the resolution of detector array and the speed of the phase measurement. Another alternative way of solving this problem is to use a longer wavelength light source. One can either use an infrared light source or use two shorter visible wavelengths to synthesize a longer equivalent wavelength as is used in two-wavelength holographic optical testing.[3–5]

This paper will focus on two methods for solving the 2π ambiguity problem. For the first method two sets of phase data (with 2π ambiguities) for λ_a and λ_b are stored in the computer which will then calculate the phase difference between pixels for a longer equivalent wavelength λ_{eq}, according to the algorithm described in the next section. Once these new phase differences

The authors are with University of Arizona, Optical Sciences Center, Tucson, Arizona 85721.

Received 2 July 1984.
0003-6935/84/244539-05$02.00/0.

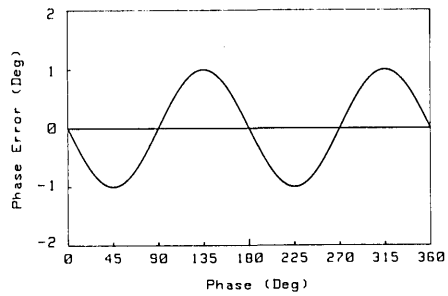

Fig. 1. Phase error vs phase for a phase step of 88° rather than 90°

between pixels are obtained, the relative wave front (OPD) plot or relative surface height plot can be obtained by integrating all the phase difference values. A typical result is included in Experiment II. In the second, more accurate method, two different wavelengths are used to solve for the 2π ambiguities and these data are used to correct for the 2π ambiguities in the single-wavelength data. The result for the second method is included in Experiment III. Using our present interferometer setup the maximum measurable wave front slope is increased by 40% at $\lambda = 6328$ Å. If one could change the setup to get better fringe visibility, the dynamic range would be better.

II. Phase Calculation Algorithm for λ_{eq}

For simplicity only the 1-D phase calculation algorithm will be shown here since the 2-D phase calculation is basically the same as that of the 1-D case. By doing separate phase measurements for λ_a and λ_b two sets of phase data are obtained: $\phi_{1a},\phi_{2a},\phi_{3a},\ldots\phi_{Na}$ for λ_a and $\phi_{1b},\phi_{2b},\phi_{3b}\ldots,\phi_{Nb}$ for λ_b, where N is the total number of pixel elements in the detector array.

Assuming an index of refraction equal to 1, the OPD values on each pixel as shown in Fig. 2 can be related to the measured phase value mentioned above by a simple relation. For example, at pixel number n we have

$$\mathrm{OPD}_n = \left[\frac{\phi_{na}}{2\pi} + m\right]\lambda_a, \tag{1}$$

or

$$\mathrm{OPD}_n = \left[\frac{\phi_{nb}}{2\pi} + p\right]\lambda_b, \tag{2}$$

where m and p are order numbers for λ_a and λ_b. Similarly, one can write equations for the next pixel:

$$\mathrm{OPD}_{n+1} = \left[\frac{\phi_{(n+1)a}}{2\pi} + m'\right]\lambda_a, \tag{3}$$

or

$$\mathrm{OPD}_{n+1} = \left[\frac{\phi_{(n+1)b}}{2\pi} + p'\right]\lambda_b. \tag{4}$$

Again m' and p' are order numbers for λ_a and λ_b on pixel number $n+1$. There is one more unknown than the equations we have, if we want to solve for the absolute OPD at every pixel. Since we are interested in relative OPDs rather than absolute OPDs, let us write the expressions for the difference of OPDs between adjacent pixels:

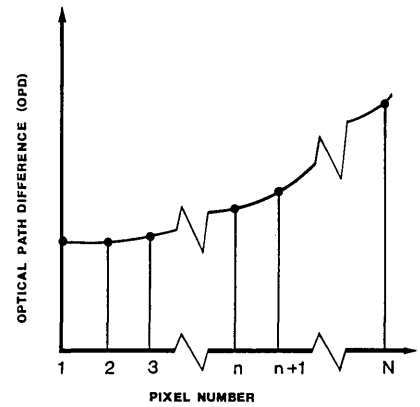

Fig. 2. Arbitrary optical path difference (OPD) distribution across the detector array.

Using Eq. (3) minus Eq. (1) we have

$$2\pi[\mathrm{OPD}_{n+1} - \mathrm{OPD}_n] = [(\phi_{(n+1)a} - \phi_{na}) + 2\pi(m' - m)]\lambda_a. \tag{5}$$

Using Eq. (4) minus Eq. (2) we have

$$2\pi[\mathrm{OPD}_{n+1} - \mathrm{OPD}_n] = [(\phi_{(n+1)b} - \phi_{nb}) + 2\pi(p' - p)]\lambda_b. \tag{6}$$

For simplicity let

$$\Delta\mathrm{OPD}_{n+1} = \mathrm{OPD}_{n+1} - \mathrm{OPD}_n,$$

$$\Delta\phi_{(n+1)a} = \phi_{(n+1)a} - \phi_{na},$$

$$\Delta\phi_{(n+1)b} = \phi_{(n+1)b} - \phi_{nb}.$$

Again, we have three unknowns, i.e., $\Delta\mathrm{OPD}_{n+1}$, $(m' - m)$, and $(p' - p)$. We need one more assumption. Assume the difference of order numbers between any adjacent pixels is the same for both λ_a and λ_b, i.e., $m' - m = p' - p = \Delta M_{n+1}$. From Eqs. (5) and (6) we can solve for ΔM_{n+1}:

$$\Delta M_{n+1} = \frac{\Delta\phi_{(n+1)b}\lambda_b - \Delta\phi_{(n+1)a}\lambda_a}{2\pi[\lambda_a - \lambda_b]}. \tag{7}$$

Substituting Eq. (7) into Eq. (5) or Eq. (6) yields

$$\Delta\mathrm{OPD}_{n+1} = [(\Delta\phi_{(n+1)b} - \Delta\phi_{(n+1)a})/2\pi](\lambda_a\lambda_b)/(\lambda_a - \lambda_b). \tag{8}$$

Rewriting Eq. (8) we have

$$\Delta\mathrm{OPD}_{n+1} = \begin{cases} \dfrac{1}{2\pi}[\Delta\phi_{(n+1)b} - \Delta\phi_{(n+1)a}]\lambda_{eq} \text{ if } \lambda_a > \lambda_b, \\ \dfrac{1}{2\pi}[\Delta\phi_{(n+1)a} - \Delta\phi_{(n+1)b}]\lambda_{eq} \text{ if } \lambda_b > \lambda_a. \end{cases} \tag{9}$$

If the assumption mentioned above is true, the difference of OPD values between any adjacent pixels can be obtained using Eq. (9). Then, simply by adding all the ΔOPDs together, the OPD distribution across the detector array can be reconstructed. Note, the fundamental assumption for the single-wavelength PSI is that the ΔOPDs between any adjacent pixels be less than $\lambda/2$. For the TWLPSI case the ΔOPDs between any adjacent pixels must be less than $\lambda_{eq}/2$. This means that, if the test were performed using a single-wavelength (wavelength = λ_{eq}) light source, the phase difference between any adjacent pixels would be $<\pi$ and no 2π ambiguity problem would occur. Under this assumption $(m' - m) - (p' - p)$ may be equal to +1 or

-1 instead of 0 depending on the relative position between detector elements and the fringe pattern imaged on the detector array. If $(m' - m) - (p' - p)$ were not equal to 0, Eq. (9) would give a wrong value of ΔOPD_{n+1} such that its absolute value would always be larger than $\lambda_{eq}/2$ and appear to violate the fundamental assumption. These discontinuities can be checked and removed by a method similar to that used in single-wavelength PSI to integrate the OPD profile across the array.

A computer simulation for TWLPSI has been performed to show that the above relationship between λ_{eq} and the wave front slope is correct. Figure 3 shows the results.

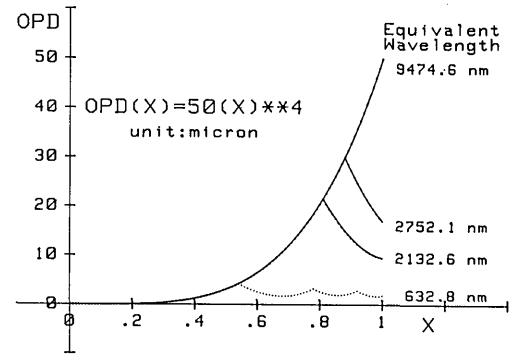

Fig. 3. Computer simulation results for TWLPSI, longer λ_{eq} is needed for a steeper wave front. For comparison, the dotted line shows results for single-wavelength PSI.

III. Sources of Error

There are several major sources of error that need to be taken care of. (1) Air turbulence: the wave front might change between taking the data set for λ_a and the data set for λ_b. (2) PZT calibration error: the error in the accuracy and linearity of the motion of the PZT used to drive the reference mirror will produce a kind of noise which has different spatial frequency for different wavelengths. (3) Data matching problem: if the phase data for λ_a and λ_b are not for the same data points, a shearing effect error will be superimposed on the measurement result. (4) Chromatic variations of wave front aberration and high frequency structure: any refractive optical element, e.g., lenses, beam splitters, will alter the ray paths slightly for different wavelengths and generate errors. (5) Extraneous fringes and speckle noise as discussed in Ref. 6. (6) Finite size of detector elements: since detector elements are not ideally point detectors, the measured phase is an averaged phase across the finite width of each detector element. Meanwhile the fringe visibility is reduced at higher spatial frequency by some amount according to the sinc function in Eq. (10); here we assume the length of the detector array is infinite:

$$V(f_x) = K[I(f_x)\,\text{sinc}(W_d f_x)] * [\text{comb}(Sf_x)], \tag{10}$$

where $V(f_x)$ is the spectrum of detected signal,
$I(f_x)$ is the spectrum of fringe pattern,
W_d is the width of detector elements,
K is a normalization factor, and
S is the spacing between detector elements.

The phase error due to the average effect mentioned above is quite small. For the detector array we are using a defocus or third-order spherical as large as 200 μm will not generate an error larger than $\lambda/1000$.

To get more insight into the effect of these errors, let us rewrite Eq. (9) and assume $\lambda_a > \lambda_b$,

$$\Delta\text{OPD}_{n+1} = \frac{1}{2\pi}[\Delta\phi_{(n+1)b} - \Delta\phi_{(n+1)a}]\left[\lambda_{eq}\Big/\left(\frac{\lambda_a + \lambda_b}{2}\right)\right]\left(\frac{\lambda_a + \lambda_b}{2}\right)$$
$$= \frac{1}{2\pi}[\Delta\phi_{(n+1)b} - \Delta\phi_{(n+1)a}]M_{ab}\left(\frac{\lambda_a + \lambda_b}{2}\right), \tag{11}$$

where M_{ab} is the wavelength magnification ratio and is defined as the ratio of equivalent wavelength over the mean wavelength for λ_a and λ_b. The difference of

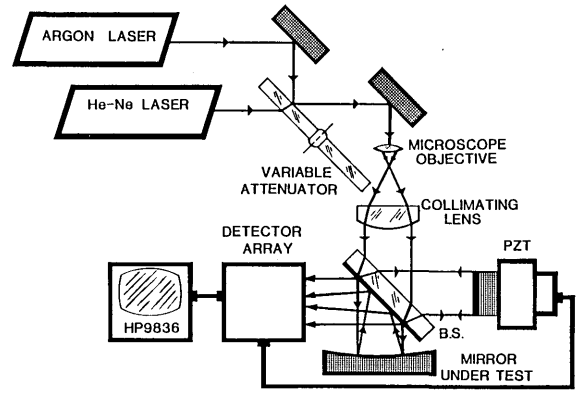

Fig. 4. Experimental setup for the TWLPSI.

phase difference $[\Delta\phi_{(n+1)b} - \Delta\phi_{(n+1)a}]$ in Eq. (11) can be separated into two terms, i.e., $[\Delta\phi_{(n+1)b} - \Delta\phi_{(n+1)a}]_S$ due to the surface under test and $[\Delta\phi_{(n+1)b} - \Delta\phi_{(n+1)a}]_E$ due to any kind of error sources that produce a nonzero value of $[\Delta\phi_{(n+1)b} - \Delta\phi_{(n+1)a}]_E$.

Then the measured OPD difference becomes

$$\Delta\text{OPD}_{n+1} = \frac{1}{2\pi}\{[\Delta\phi_{(n+1)b} - \Delta\phi_{(n+1)a}]_S + (\Delta\phi_{(n+1)b} - \Delta\phi_{(n+1)a})_E\}$$
$$\times M_{ab}\left(\frac{\lambda_a + \lambda_b}{2}\right). \tag{12}$$

From Eq. (12) it is clear that the $[\Delta\phi_{(n+1)b} - \Delta\phi_{(n+1)a}]_E$ term (ideally it should equal zero) will be amplified by a factor of M_{ab}, adding to the true data. This error magnification effect looks like a common disadvantage for all two-wavelength techniques.

IV. Experiments

The experimental setup is shown in Fig. 4. This particular experimental arrangement was used because it provided a convenient means of obtaining high frequency interference fringes needed to test the two-wavelength measurement technique. An argon-ion laser and a He–Ne laser were used as the light sources. The reference mirror and spherical mirror were put as close to the beam splitter as possible to reduce air turbulence problems. There was no diverging lens used

Table I. Error (e.g., High Frequency Noise) Amplification Effect of the Equivalent-Wavelength Phase Calculations for Different λ_{eq}

$\lambda_{eq}(\mu m)$	6.45	9.47	11.83	14.19	20.22	28.5
Measured value rms (Å)	200.4	255.5	343.8	366.8	534.9	726.7
Estimated value rms (Å)	203.6	254.7	346.6	367.4	539.6	725.1

in the setup in order to reduce chromatic problems and to get more fringes. The imaging lens was also taken out in Experiments II and III to remove aberrations introduced by the lens. The diffraction effect could be reduced if the measurement region were away from the edge of the aperture. Since a spherical wave front is being measured, the beam splitter will cause only tilt error even though the fringe pattern is sheared a little for the second wavelength. Fringe patterns are sampled by a Reticon RC1728H linear array (only 1024 pixels being used); the analog signal is then converted into a 10-bit digitized signal which is fed into a HP9836 microcomputer for processing.

A. Experiment I

In this experiment the effect of error (e.g., high frequency noise) amplification was examined. The spherical mirror was replaced by a plane mirror so that tilt fringes could be removed. Since four laser lines, 5145, 4965, 4880, and 4765 Å, were used in this experiment, we can have six equivalent wavelengths. The rms value of the two-wavelength measurement has a nearly linear dependence on λ_{eq} as shown in Table I. These measured values are also in good agreement with those estimated by simply finding out the rms difference between single-wavelength measurement for λ_a and λ_b then multiplying by a magnification factor M_{ab}.

B. Experiment II

In this experiment the spherical mirror was replaced to produce a deep defocused wave front with a wave front sag of ~200 μm (remember there is a factor of 2 between surface height and wave front). To reduce the effect of error magnification, the 6328-Å laser line of a He–Ne laser was used in combination with the laser lines of an argon-ion laser. The wave front slope was steep enough (~800 waves across the array) to break the limitation for single-wavelength PSI as shown in Fig. 5(a) for λ = 6328 Å and Fig. 5(b) for λ = 5145 Å. Figure 5(c) shows the equivalent-wavelength (λ_{eq} = 2.75 μm) surface height data and proves that TWLPSI is working to reconstruct a steep wave front. Figure 5(d) shows the same data as in Fig. 5(c) but with both tilt and focus subtracted out. The repeatability of this measurement by the first method of TWLPSI without temporal averaging is ~130-Å rms.

C. Experiment III

In this experiment, the second method proved effective. Since the equivalent-wavelength phase data generated by the two-wavelength algorithm are more noisy than those input single-wavelength phase data, the best solution is using the equivalent-wavelength

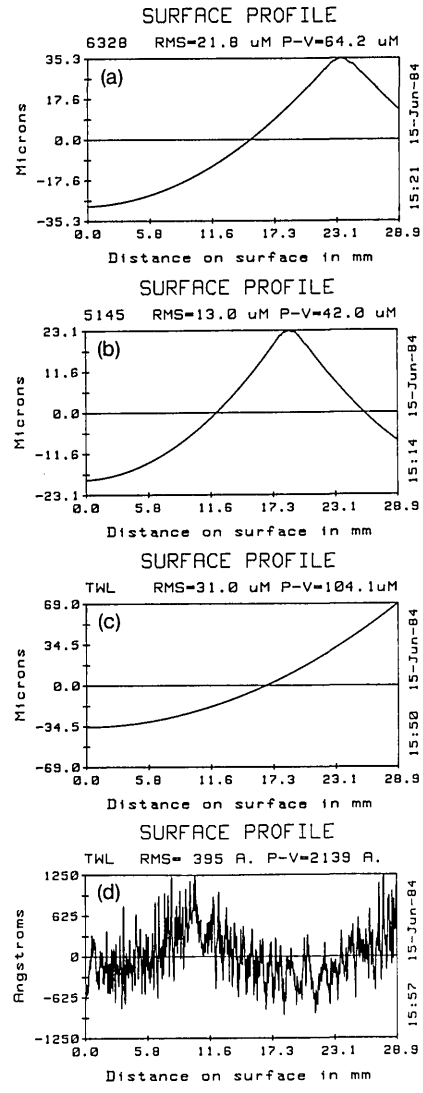

Fig. 5. (a) Single-wavelength data obtained at λ = 6328 Å showing breakdown of phase measurement when the wave front slope is too steep. (b) Similar data as in (a) but λ is changed to 5145 Å. (c) The equivalent wavelength (λ_{eq} = 2.75 μm) data. (d) Same data as in (c) but with both tilt and focus removed.

phase data as a reference to correct 2π ambiguities in the single-wavelength phase data for either λ_a or λ_b. Once the noise in the equivalent-wavelength phase data is small enough, the 2π ambiguity correction is quite successful. Figure 6 shows results of the corrected single-wavelength surface height measurement data for λ = 6328 Å and λ = 5145 Å. This ability of 2π ambiguity correction looks like the true potential of the

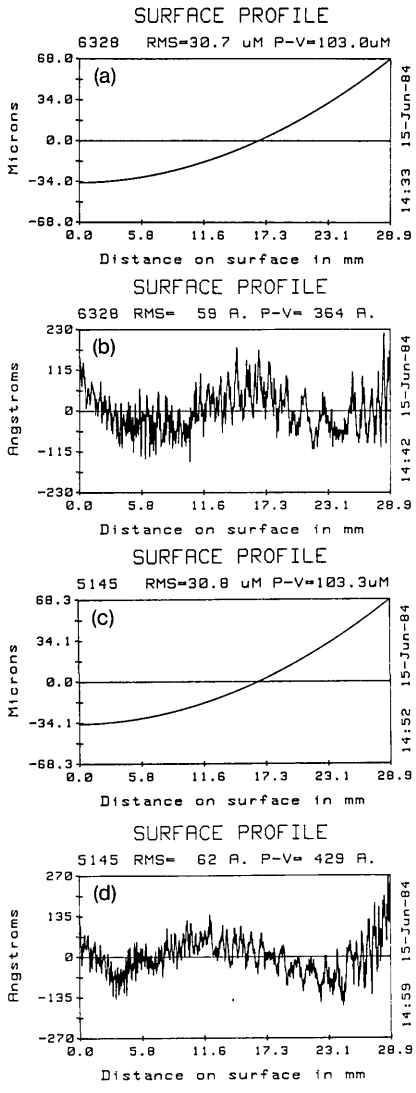

Fig. 6. (a) Single-wavelength data obtained at $\lambda = 6328$ Å with 2π ambiguities corrected. (b) Same data as in (a) but with both tilt and focus removed. In (c) and (d) the wavelength was changed to 5145 Å.

TWLPSI and makes the precision (repeatability) of the surface height measurement better than 25-Å rms (0.0025%) as shown in Fig. 7(a). Figure 7(b) shows the

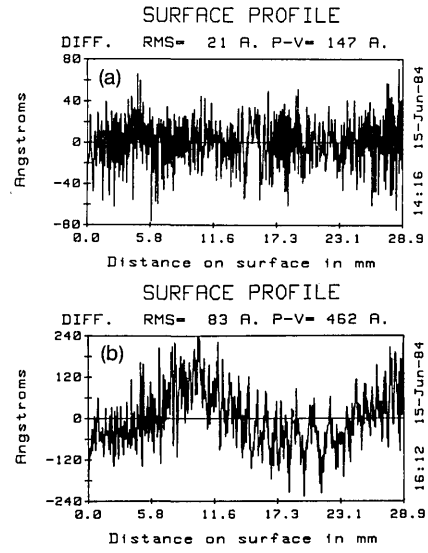

Fig. 7. (a) Repeatability of the surface height measurement without temporal averaging by the second method of TWLPSI (obtained at $\lambda = 6328$ Å). (b) Difference between the data sets in Fig. 6(b) ($\lambda = 6328$ Å) and Fig. 6(d) ($\lambda = 5145$ Å).

difference between the single-wavelength data shown in Figs. 6(b) and (d). The noise amplification effect becomes clear when one compares it with Fig. 5(d).

V. Conclusion

In conclusion, a high precision technique for testing of steep optical surfaces has been developed. Since all the necessary phase calculations have been done inside a computer, no hologram is required as in two-wavelength holography. A sample test measuring the surface height of a spherical mirror without a diverging lens (wave front sag = 200 μm) has been performed to verify the capability of the TWLPSI. The precision of the measurement without temporal averaging is better than 25-Å rms. Possible applications of the TWLPSI are in the testing of steep aspheric surfaces or in the area of active optics where surface deformations are very large.

References

1. J. H. Bruning, "Fringe Scanning Interferometers," in *Optical Shop Testing*, D. Malacara, Ed. (Wiley, New York, 1978).
2. C. Koliopoulos, "Interferometric Optical Phase Measurement Techniques," Ph.D. Dissertation, Optical Sciences Center, U. Arizona (1981).
3. B. P. Hildebrand and K. A. Haines, "Multiple-Source Holography," J. Opt. Soc. Am. **57,** 155 (1967).
4. C. Polhemus, "Two-Wavelength Interferometry," Appl. Opt. **12,** 2071 (1973).
5. J. C. Wyant, "Testing Aspherics Using Two-Wavelength Holography," Appl. Opt. **10,** 2113 (1971).
6. J. Schwider, R. Burow, K.-E. Elssner, J. Grzanna, R. Spolaczyk, and K. Merkel, "Digital Wave-Front Measuring Interferometry: Some Systematic Error Sources," Appl. Opt. **22,** 3421 (1983).